CANADIAN APPLIED
MATHEMATICS QUARTERLY
Volume 8, Number 4, Winter 2000

MODELING EQUATOR-CROSSING CURRENTS ON THE OCEAN BOTTOM

PAUL F. CHOBOTER AND GORDON E. SWATERS

ABSTRACT. Observations unambiguously show that deep ocean currents carry a significant amount of fluid across the equator. Away from the equator in either hemisphere, these currents are relatively quiescent so that planetary vorticity dominates relative vorticity within the fluid. Thus, the potential vorticity of cross-equatorial flow changes sign en route. The breakdown of geostrophic balance at the equator because of the vanishing horizontal component of the Coriolis force and the fact that potential vorticity is not conserved in these flows constitute formidable challenges to modeling these cross-equatorial currents.

Recent research points to friction as being crucial to the crossing process since it provides the mechanism by which potential vorticity can be altered. As well, since these flows are bottom-dwelling currents, the geometry of the bottom topography is an important factor in determining the portion of the current which successfully crosses the equator.

We examine the dynamical balances within equator-crossing flows by studying a simplified model of the flow in the equatorial region. This model retains the effects of friction and bottom topography. We compare the predictions of this model with the predictions of more sophisticated numerical models and with observations. It is shown that, despite the simplicity of the model, it captures certain aspects of the flow quite well.

1. Introduction. Abyssal flows, as part of the global thermohaline circulation, make a significant contribution to the flux of heat over the earth, and therefore affect the planet's climate. In the Atlantic, the deepest flow consists of Antarctic bottom water, which originates in the Weddel Sea near Antarctica and flows northward along the western boundary of the Atlantic ocean. While part of this flow recirculates within the Brazil Basin, remaining in the southern hemisphere, part of the flow is observed to cross the equator into the northern hemisphere, Figure 1. See also [**4, 8**].

Preparation of this paper was supported in part by a Killam Postgraduate Scholarship awarded to the first author and a research grant awarded to the second author by the Natural Sciences and Engineering Research Council.

Like many mesoscale and large-scale flows in the atmosphere and ocean, these abyssal flows are observed to be geostrophically balanced, to leading order, away from the equator. Indeed, many models of motion on these scales are derived by assuming the leading-order velocity fields are geostrophic, [**11**]. However, geostrophy must necessarily break down in the vicinity of the equator, since the Coriolis parameter $f = 2\Omega \sin\theta$, where Ω is the earth's angular velocity and θ is latitude, vanishes at the equator.

Potential vorticity, $q = (f+\zeta)/h$ in the shallow-water approximation, where $\zeta = \mathbf{k} \cdot \nabla \times \mathbf{u}$ is the vertical component of the relative vorticity and h is the depth of the layer, is exactly conserved following the flow if friction effects are neglected.

However, the fluid in these abyssal flows is relatively quiescent before and after crossing the equator; that is, planetary vorticity dominates relative vorticity, when sufficiently far from the equator, so that $q \approx f/h$. Therefore, since $f < 0$ in the southern hemisphere and $f > 0$ in the northern hemisphere, the potential vorticity of the fluid has changed sign and so is certainly not conserved. This violation of potential vorticity conservation in cross-equatorial flows, as well as the breakdown of geostrophy at the equator, make these flows interesting to study and a challenge to model.

Edwards and Pedlosky [**6**] examined potential vorticity modification in nonlinear equator-crossing currents. They modeled the equatorial ocean with a one-layer shallow water model, assuming a flat bottom topography and horizontal friction. They forced fluid across the equator by specifying a localized mass source in the northern hemisphere and a distributed mass sink in the southern hemisphere. The equations of motion were integrated numerically in a number of simulations, and vortices were observed to develop as the fluid approaches the equator, particularly for the more strongly forced runs. An analysis of the vorticity flux showed that the eddy field transports vorticity to the side boundary, where friction dissipates the vorticity. They concluded that, for cross-equatorial flow to occur, the eddy field must work in conjunction with the dissipative side layer to modify the vorticity. In a linear stability analysis of a steady meridional current, Edwards and Pedlosky [**7**] showed that the instability is essentially an inviscid shear instability so that, although friction is necessary for potential vorticity modification, it does not play a role in the production of the eddies

which transport the potential vorticity to the side boundary.

Nof and Olson [**17**] pointed out that the northward-flowing Antarctic bottom water is observed to flow along the left flank of the ocean basin, i.e., closest to the continent, as it approaches the equator, but flows along the right flank of the ocean basin, i.e., next to the mid-Atlantic ridge, after crossing the equator. They proposed that simple geostrophy requires that the current can only cross the equator if it switches sides of the basin as it crosses. To support this conclusion, they analytically solved two steady, inviscid reduced-gravity models: a 1-1/2 layer model in a parabolic meridional channel, and a 2-1/2 layer model with flat topography, where the current had constant potential vorticity. The solutions showed that the equator is successfully crossed, and that the bottom current does switch sides. We note that Johnson [**10**] also studied a steady, inviscid, reduced-gravity model with a constant potential vorticity flow, but with a linear bottom topography, and found that the current crossed the equator by adjusting its width and height as it crossed.

Kawase, Rothstein and Springer [**12**] numerically integrated the three-dimensional equations of motion, specifically the Boussinesq, hydrostatic, incompressible equations in spherical coordinates, over a domain centered on the equator. Although they employed the full equations of motion, they neglected bottom topography and the geometry of the side boundaries. They observed a southern flowing deep western boundary current as it approached the equator. During the initial spin-up stages, the current turns eastward along the equator but, in the steady-state limit, the current crosses the equator along the western boundary, where the flow is most nonlinear.

Borisov and Nof [**2**] suggested that deep currents may cross the equator in the form of eddies and, as a result, studied the dynamics of eddies approaching the equator in a parabolic meridional channel. They first studied the dynamics of solid, frictionless, noninteracting particles in the channel and obtained statistics showing the likelihood of a given particle to cross the equator when its initial position and velocity are known. They then employed a one-layer reduced-gravity shallow water model and performed numerical experiments on eddies approaching the equator. The portion of the eddy crossing the equator was found to depend on the geometry of the channel and the initial speed and direction of the eddy. The presence of friction alters the

potential vorticity of the eddy to allow some of the fluid to cross the equator, but the portion of the fluid which crossed was found to be more dependent on geometry than on potential vorticity modification.

Nof and Borisov [**16**] compared the numerical simulations of double frontal currents on a parabolic meridional channel using a reduced-gravity shallow-water model to the solid particles of Borisov and Nof [**16**] and to the analytic solution of Nof and Olson [**17**]. Since the shallow-water simulations compared favorably with the dynamics of the solid particles, Nof and Borisov [**16**] concluded that the equator-crossing process is an inertial one where the geometry of the bottom topography plays a crucial role. The differences between the inviscid analytic solutions of Nof and Olson [**17**], where potential vorticity is conserved, and the viscous shallow water simulations led them to conclude that the potential vorticity is modified by friction as the current proceeds, allowing the flow to propagate along the path prescribed by the bottom topography.

Stephens and Marshall [**21**] studied the movement of abyssal waters in the Atlantic by numerically integrating a simple model of bottom-layer flow where the full shallow water conservation of mass equation was retained (with a small sink term representing the effects of upwelling), but the momentum equations were replaced by a planetary geostrophic approximation with the addition of Rayleigh friction. This model was integrated using realistic topographic data, and the resulting steady flow was found to be broadly consistent with observations.

The frictional geostrophic model employed by Stephens and Marshall [**21**] is appealing in the sense that it includes frictional effects, allows the flow to be steered by topography, and supplies a diagnostic relation for the velocity field in terms of the pressure field which, unlike the usual geostrophic relations, remains valid even at the equator. However, how appropriate this model is for these flows has not been established. Our goal here is to compare the frictional geostrophic model to the more realistic shallow-water equations to identify to what extent the model captures the essential physics of the problem.

We caution that the reduced-gravity shallow-water model is itself a crude approximation to the dynamics associated with abyssal currents. Neglected effects include turbulent entrainment, vertical overturning and baroclinic effects. Possible improvements to the model include

employing several shallow layers to mimic an isopycnal coordinate system. We also caution that, as shown by Colin de Verdière and Schopp [**3**], the "horizontal component" of the Coriolis force, which is neglected as part of the hydrostatic approximation, may be important in equatorial dynamics, particularly if the horizontal length scales of motion are smaller than $(Ha)^{1/2}$, where H is a vertical scale of the motion and a is the radius of the earth. For a vertical scale of $H = 200$ m, this length scale is on the order of 40 km, which is smaller than the $O(500$ km) length scales we study here, so the traditional approximation is retained.

The plan of the paper is as follows. In Section 2 we present the simple model. In Section 3 the dynamics of the simple model are compared with the dynamics of the reduced-gravity shallow-water model. We provide some concluding remarks in Section 4.

2. Frictional geostrophic model. Models in which the momentum equations have been reduced to the geostrophic relations with the addition of a linear term representing the effects of friction have been used to study various large-scale motions by several authors, see [**21, 5, 19, 20**] and references therein. Pedlosky [**18**], see also [**21, 13**], showed that the effect of a bottom Ekman layer is equivalent to the effect of linear Rayleigh friction with a coefficient $r = (\nu_z f/2)^{1/2}/h = f\delta_E/2h$ where ν_z is a vertical eddy viscosity coefficient, f is the Coriolis parameter, δ_E is the Ekman layer thickness and h is the layer thickness. This expression for r implies that $r \to 0$ at the equator. In order to retain the effect of nonzero friction at the equator, Stephens and Marshall [**21**] neglect the dependence of r on f, but retain the h dependence. However, Edwards et al. [**5**], Samelson [**19**] and Samelson and Vallis [**20**] all neglected the h dependence as well, taking r to be a prescribed constant. For simplicity, we will take r to be a prescribed constant in this study.

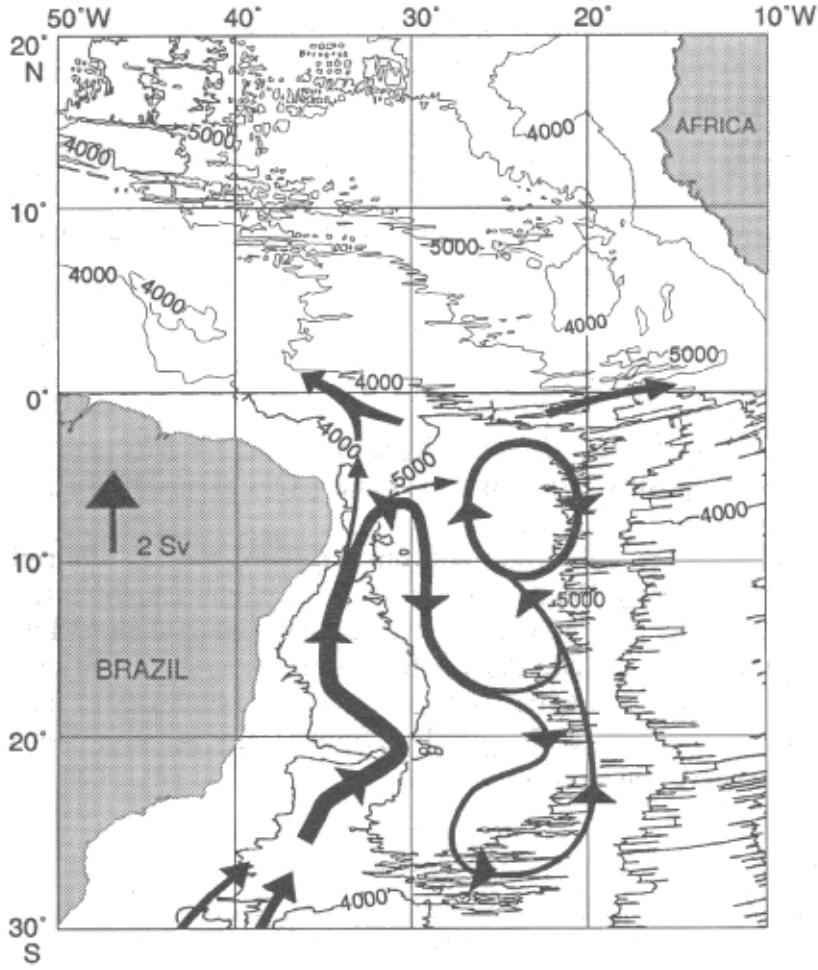

FIGURE 1a). Schematic of path of Antarctic bottom water in the southern Atlantic ocean, based on observations. 1 Sv = 10^6 m^3 s^{-1}

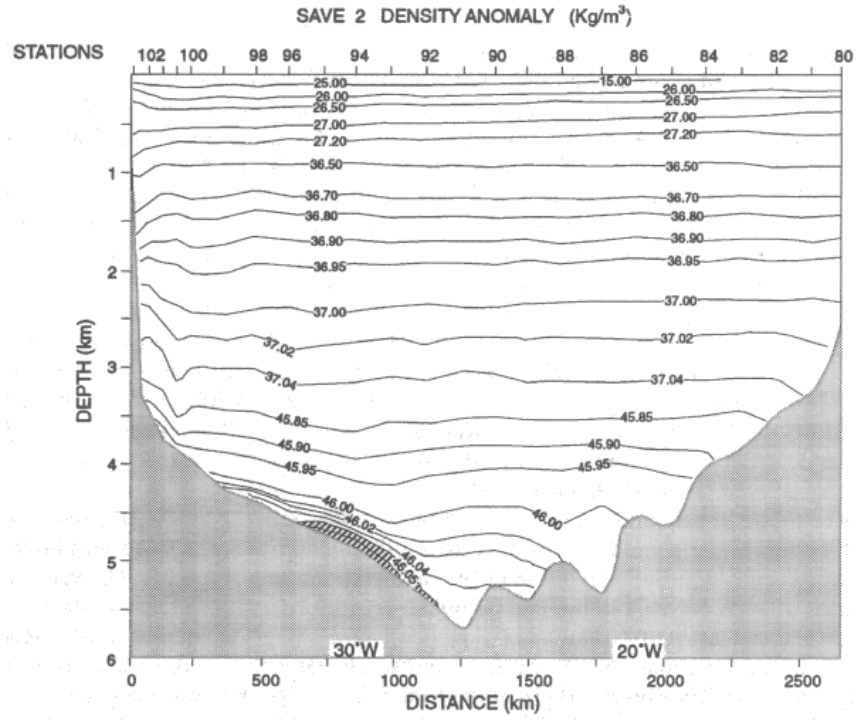

FIGURE 1b). Density data at 20°S showing the cross section of the core of the Antarctic bottom water, shaded. Both figures are as they appear in Nof and Borisov [**16**], modified from DeMadron and Weatherly [**4**]..

The model equations may then be written in the form

$$-fv = -\frac{\partial(h + h_B)}{\partial x} - ru, \tag{1}$$

$$fu = -\frac{\partial(h + h_B)}{\partial y} - rv, \tag{2}$$

$$\frac{\partial h}{\partial t} + \nabla \cdot (h\mathbf{u}) = 0, \tag{3}$$

where $\mathbf{u} = (u, v)$ is the horizontal velocity with u the eastward velocity and v the northward velocity, x and y are the eastward and northward coordinates, respectively, h is the height of the fluid layer, h_B is the bottom topography elevation, f is the Coriolis parameter, and r is a damping coefficient to be specified. Note that (1)–(3) are in

nondimensional form, with $r = r_0/f_0$, where r_0 and f_0 are typical dimensional values for r and f, respectively. The remaining variables are scaled exactly as for the shallow-water equations, as discussed in Section 3.1. Assuming that (1) and (2) have the advantage of allowing the velocities u and v to be solved for in a *diagnostic* relation in terms of the pressure gradients,

$$u = \frac{-fp_y - rp_x}{f^2 + r^2}, \quad v = \frac{fp_x - rp_y}{f^2 + r^2}, \tag{4}$$

where $p = h + h_B$ and subscripts denote partial derivatives. Thus, the model contains a geostrophic component (terms proportional to f in the numerator), and a down-pressure gradient component (terms proportional to r in the numerator). In the limit as $f \to 0$, the motion is that of a potential flow. Note that frictional effects prevent the unbounded acceleration of the fluid downhill, since the downhill component may be interpreted to represent the terminal velocity that the fluid would attain when acceleration and friction effects are in balance at steady state.

The model may be written as a single evolution equation for the height field, h, by substituting the velocity relations (4) into the conservation-of-mass equation (3),

$$h_t + J\left(h + h_B, \frac{hf}{f^2 + r^2}\right) = r\nabla \cdot \left[\frac{h\nabla(h + h_B)}{f^2 + r^2}\right], \tag{5}$$

where $J(A, B) = A_x B_y - A_y B_x$. This form of the model reveals that, despite its simplicity, it is a nonlinear model. As well, it is clear that r determines how diffusive the model will be, since it multiplies the diffusion-type operator on the right-hand side of the equation.

The potential-vorticity equation of this model is

$$\frac{\partial}{\partial t}\left(\frac{f}{h}\right) + \mathbf{u} \cdot \nabla\left(\frac{f}{h}\right) = -\frac{r}{h}\zeta, \tag{6}$$

where $\zeta = v_x - u_y$ with u and v given by (4). This model, then, effectively neglects relative vorticity in favor of planetary vorticity and has the feature that it simulates the dissipation of potential vorticity by Ekman friction. In the limit as $r \to 0$, f/h is conserved following the

flow. This limiting state implies that, for $0 < r \ll \max|f|$, a mass of fluid approaching the equator will tend to decrease in height, since $|f|$ decreases as the equator is approached. This process continues until the righthand side of (6) becomes non-negligible, which occurs when $r/h \sim O(1)$ (nondimensional values). This represents the point at which the effects of friction will be dynamically important. Assuming h and f to be $O(1)$ initially, frictional effects will thus be important at a latitude where $f = O(r)$, i.e., at a nondimensional distance from the equator of r/β, where $\beta = df/dy$ at $y = 0$.

A consequence to the form of (4) is that the component of velocity parallel to the pressure gradient is necessarily in the direction opposite to that gradient. That is,

$$\mathbf{u} \cdot \nabla p \leq 0, \tag{7}$$

which follows directly from the fact that (4) implies $\mathbf{u} \cdot \nabla p = -r^2|\nabla p|^2/(r^2 + f^2)$.

The major disadvantage of this model is its oversimplification of the dynamics. For example, fluid inertia has been neglected. Since the fluid may never move up the pressure gradient, a mass of fluid flowing down one side of a valley does not have the momentum to flow back up the other side.

It is not expected that this model will reproduce the detailed dynamics within the equatorial region. The model will be evaluated on its ability to predict the *net* effect on a geostrophically balanced flow as it passes through the equatorial region and emerges on the other side or recirculates, again geostrophically balanced.

3. Frictional geostrophic versus shallow water.

3.1 *Numerical methods.* We numerically integrate forward in time the reduced-gravity shallow water model (8)–(9) below, and the frictional geostrophic model (1)–(3) in order to compare the two models. The shallow water model may be written in nondimensional form as

$$\frac{\partial \mathbf{u}}{\partial t} + \mathbf{u} \cdot \nabla \mathbf{u} + \frac{f}{Ro}\mathbf{k} \times \mathbf{u} = -\frac{1}{Ro}\nabla(h + h_B) + \mathbf{F}_{\mathbf{fric}}, \tag{8}$$

$$\frac{\partial h}{\partial t} + \nabla \cdot (\mathbf{u}h) = 0 \tag{9}$$

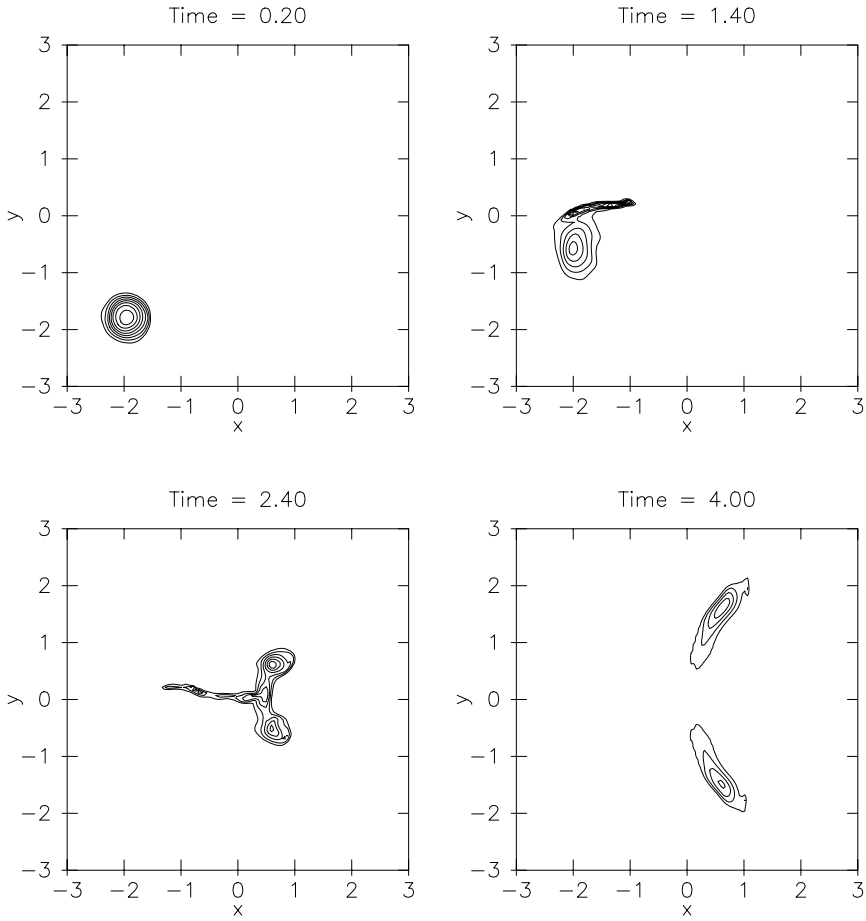

FIGURE 2. The results of a shallow water simulation, $Ro = 0.02$. The contour spacing is 0.02. x and y are nondimensional east-west and north-south coordinates, respectively. $x = 0$ is the deepest part of the channel, and $y = 0$ is at the equator.

where $\mathbf{u}$ is the horizontal velocity vector, $\mathbf{F_{fric}}$ represents the friction term, $Ro = U/f_0L$ is the Rossby number and U, L, f_0 and h_0 are typical scales for the velocity, length, Coriolis parameter and fluid depth, respectively. It has been assumed that the time variable is scaled advectively, $T = L/U$ for a time scale T, and that the scale slope for the bottom topography is the same as the scale slope of the fluid height, h_0/L. We have also employed the geostrophic scaling $U^2/(g'h_0) = Ro$. (This implies $Ro = Fr^2$, where Fr is the Froude number.) Since f passes through zero in the domain of interest, f_0 is taken to be the dimensional value of f at a latitude away from the equator where the flow is geostrophic.

These equations are discretized on an Arakawa C-grid, [**1**]. The spatial discretization of the advection, Coriolis and pressure gradient terms is performed using the scheme of Arakawa and Hsu [**1**]. This scheme, which is designed to tolerate an arbitrarily small layer thickness, i.e., intersections of the fluid surface with the bottom topography, conserves energy and weakly dissipates potential enstrophy when the mass flux is nondivergent. It is a second-order accurate scheme.

The temporal discretization of the momentum equations is according to a third-order accurate scheme by Matsuno [**14**]. It is equivalent to a third-order Runge-Kutta method.

The mass equation is stepped forward in time using the method of Hsu and Arakawa [**9**], which is a predictor-corrector scheme second-order accurate in time and space that maintains the positive-definiteness of the height field h and conserves mass.

We have taken friction to be in the form

$$\mathbf{F_{fric}} = A_H\nabla^2\mathbf{u} + A_N\nabla^6\mathbf{u} - Av\frac{\mathbf{u}}{h^2}, \tag{10}$$

where A_H, A_N and A_V are the "horizontal," "numerical" and "vertical" friction coefficients, respectively. For the simulations reported here, $A_H = 10^{-5}$, $A_N = 10^{-9}$ and $A_V = 4 \times 10^{-8}$, unless otherwise noted. The horizontal friction term is intended to represent the effects of horizontal diffusion of momentum by subgridscale eddies. The numerical and vertical friction terms are added for numerical stability. Numerical friction effectively removes small-scale features and vertical friction is added only to prevent the aphysical acceleration of massless grid points. The horizontal and numerical terms are evaluated at each

of the three time levels in the Matsuno [**14**] scheme, but the vertical term is fully implicit at each time step.

To integrate the simple model numerically, the same routine as for the full shallow-water equations is used for the mass equation but, since there is no time derivative to evaluate in the velocity relations (4), these are simply evaluated at each time step using central differences for the derivatives.

The simple model and the shallow-water model are compared for flow over simplified bottom topography. The topography takes the shape of a meridional channel, see Figure 1. Simulations were performed with the fluid initially south of the equator, flowing northward along the western half of the channel, in the form of an eddy, i.e., the height field initially has compact support in the domain. These initial conditions were chosen, in part, to simulate the Antarctic bottom water flow, which is directed northward along the western slope toward the equator, see Figure 1.

Nof [**15**] found that the steady, frictionless motion of an isolated, relatively dense mass of a shallow fluid on a sloping bottom in a rotating system is along the slope with a constant speed that does not depend on the shape of the dense fluid or its internal velocity field. This speed, henceforth referred to as the "Nof speed," is $g's/f$, where s is the bottom slope and g' is the reduced gravity. We are interested in diagnosing how well the propagation speed of the eddy in our simulations agrees with the Nof speed. A nearly constant bottom slope and Coriolis parameter away from the channel bottom and equator facilitate computing this diagnostic. Therefore, the bottom topography is chosen to be a simplified meridional channel of hyperbolic cross section, $h_B = \sqrt{x^2 + 1}$, which has a slope approaching ± 1 away from $x = 0$, and the Coriolis parameter is chosen to be $f = \tanh(\beta_0 L y / f_0)$, which tends to a nondimensional f-plane value of unity away from $y = 0$ and has a slope at $y = 0$ of $\beta_0 L / f_0$. For simulations reported here, $\beta_0 L / f_0 = 1$, which, for f_0 evaluated at 5° latitude, corresponds to choosing a horizontal length scale of $L = 500$ km.

3.2 *Results.* Several simulations of an isolated abyssal dome of fluid approaching the equator from the south have been carried out varying only the damping parameter r in the case of the simple model, or

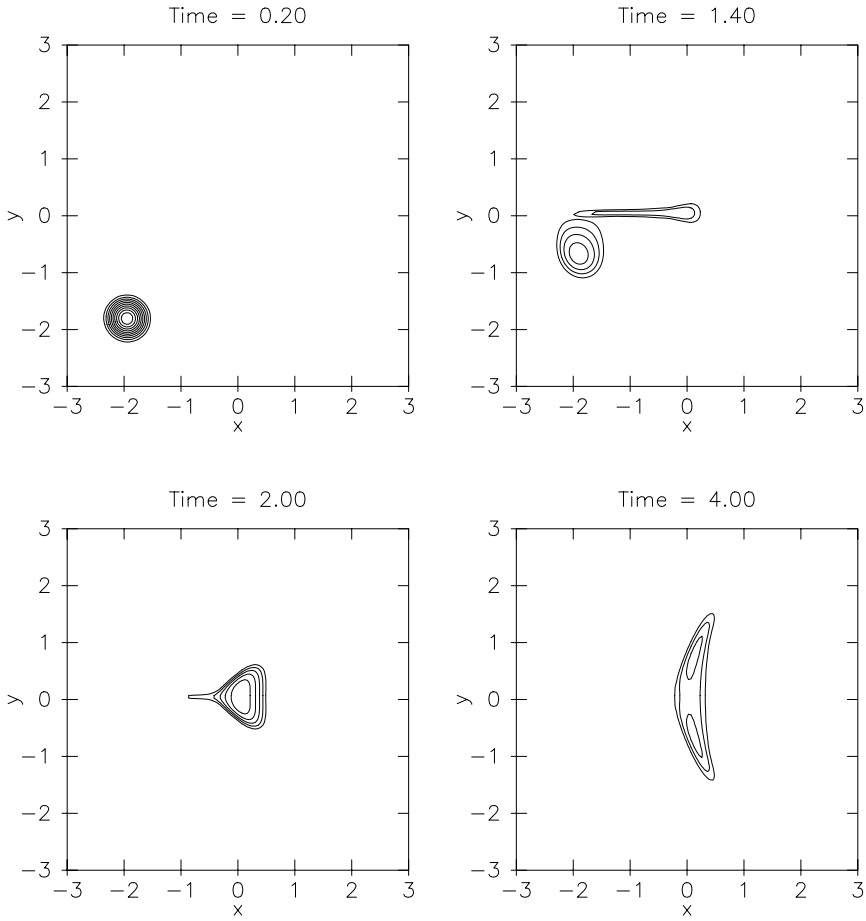

FIGURE 3. The results of a frictional geostrophic simulation, $r = 0.02$. The contour spacing is 0.02. x and y are nondimensional east-west and north-south coordinates, respectively. $x = 0$ is the deepest part of the channel, and $y = 0$ is at the equator.

the Rossby number Ro in the case of the shallow-water model. In Figure 2, we show snapshots from a typical simulation employing the shallow-water equations. The eddy is observed to propagate along the shelf without losing much height until almost at the equator, when fluid starts to accelerate downhill. Part of the fluid is located slightly north of the equator while flowing downhill. The fluid rises up the other side of the channel and ultimately splits into two eddies, one flowing northward and the other southward. This pattern is qualitatively consistent with the simulations of Borisov and Nof [**2**], who investigated eddies crossing the equator in a meridional channel.

Figure 3 displays the simulation of the motion of the same initial eddy, but as predicted by the simple model. The eddy is seen to travel initially along the slope, as in the shallow-water simulation but, upon reaching the equator, flows directly downhill, with very little fluid found north of the equator as it does so. The fluid pools at the bottom of the channel at the equator and then proceeds to split into two parts: one flows to the north and the other flows back to the south. Despite the simplicity of the model, it captures the characteristic splitting of the fluid into northward and southward-flowing parts seen in the shallow-water simulation. The lack of inertia in the model is seen in both the sharp turn from along-slope flow to downhill flow and the immediate deceleration from fast downhill flow to nearly stationary fluid pooling at the equatorial channel bottom. Thus, the net result of the lack of inertia in the model is that the north-south splitting of the flow is very symmetric, and that the final flow is very near the bottom of the channel.

We calculate the center of mass of fluid in the domain at each time for the different runs performed and display the evolution of the center of mass with time in Figure 4. One may see from the x-coordinate of the center of mass versus time plot that, for $r = 0.02$, the eddy propagates primarily along the shelf with almost no downhill motion, then suddenly accelerates in the downhill direction. For higher values of r, the downslope motion is greater initially and the maximum downhill velocity is lower. For all the simple-model runs, the fluid does not flow as high onto the opposite bank as for the shallow-water runs. This flow pattern further points to the lack of fluid inertia in the simple model. The y-coordinate center of mass versus time plot shows that the initial propagation speed along the shelf of all the runs agrees well with the

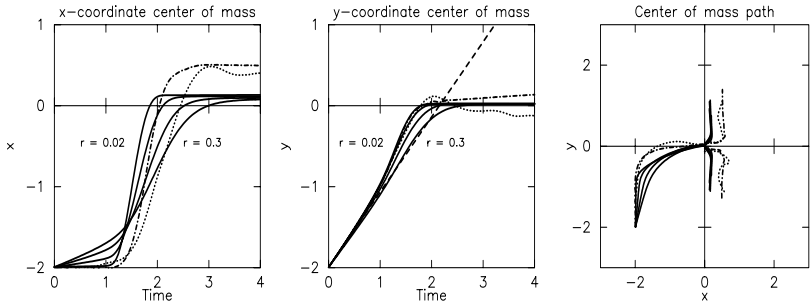

FIGURE 4. Center of mass motion. Solid lines correspond to the simple model, $r = 0.02, 0.1, 0.2, 0.3$. Dash-dot lines: SWE, $Ro = 0.02$. Dotted lines: SWE, $Ro = 0.1$. Dashed line is the slope with which an eddy moving with the Nof [**17**] speed would move.

Nof [**15**] speed. To reveal the splitting of the fluid after passing the equatorial bottom of the channel, we compute three centers of mass: the overall center of mass location, the center of mass of fluid in the northeastern quadrant of the domain, and the center of mass of fluid in the southeastern quadrant. We display in the x-versus-y plot in Figure 4 the center of mass of the entire fluid in the western half of the channel but, in the eastern half of the channel, we display the center of masses of fluid each of the northeastern and southwestern quadrants of the domain.

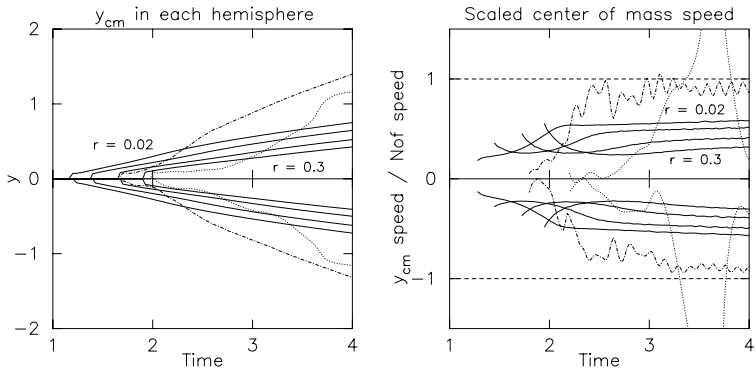

FIGURE 5. Motion after splitting. Solid lines correspond to the simple model, $r = 0.02, 0.1, 0.2, 0.3$. Dash-dot lines: SWE, $Ro = 0.02$. Dotted lines: SWE, $Ro = 0.1$. The simple model underestimates the Nof speed since it behaves more as a current than an eddy after crossing the center of the topography.

The plots in Figure 5 show diagnostics of the motion after the fluid has reached the bottom of the channel and split into northward and southward-flowing parts. The motion predicted by the simple model is seen to be quite steady in time as compared with the shallow-water model. In the plot of center-of-mass speed as compared to the local Nof speed, the shallow-water simulation with low Rossby number is seen to agree well with the theoretical speed. The higher Rossby number flow is highly variable in time, and so it is difficult to say whether or not it moves with the predicted speed in the long-term time-mean case or not. The model predicts that the center of mass of the flow propagates at a rate slower than the Nof speed for all damping parameters shown. In this way the fluid becomes more like a current than an isolated cold dome after splitting into northward and southward components.

Figure 6 displays the fraction of the total fluid residing in either hemisphere for $x \geq 0$ as a function of time. The simple model seems consistently to predict a very symmetric north/south splitting of the current. The shallow-water model does not predict a perfectly symmetric splitting, as the higher Rossby number flow has slightly more fluid recirculating south than flowing north, and vice versa for the lower Rossby number flow.

4. Discussion. The model studied here parameterizes frictional and other ageostrophic effects into a simple Rayleigh damping term. This model has been used in studies of large-scale flow, including abyssal equator-crossing flow. We have investigated the viability of this model by comparing its predictions to the predictions of shallow-water theory. Despite the simplicity of the model, it broadly captures certain aspects of shallow water flow quite well.

It remains for future work to find a suitable simplified model for equator-crossing flows. We believe a model based upon the two-layer shallow-water equations would capture more of the relevant dynamics than does the one-layer reduced-gravity model. It is desirable that a model valid at the equator reduce, in the limit of motion far from the equator, to the appropriate geostrophic model. Karsten and Swaters [**11**] derived and classified all the possible geostrophic models derivable from two-layer shallow-water theory and found that the appropriate one in the case where the lower layer is shallow and the bottom topography plays an important dynamical role is the model derived by Swaters and

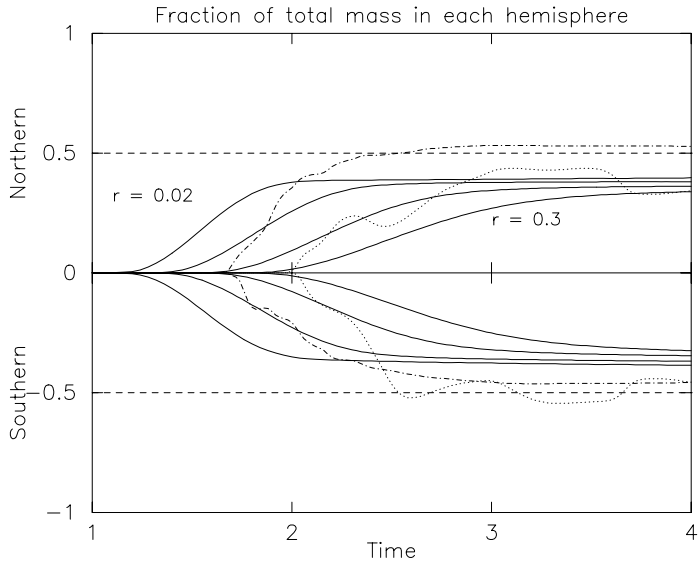

FIGURE 6. Amount of fluid in each hemisphere after splitting. Solid lines correspond to the simple model, $r = 0.02, 0.1, 0.2, 0.3$. Dash-dot lines: SWE, $Ro = 0.02$. Dotted lines: SWE, $Ro = 0.1$. The simple model predicts a symmetric splitting due to lack of fluid inertia in the model.

Flierl [**22**].

It would be possible to extend that model to the equator if diagnostic relations for velocity in terms of pressure were found that were a suitable approximation at the equator to the equations of motion in each layer. The model studied here is one candidate for such a relation for the lower layer. However, bottom friction playing a leading-order role in the dynamics of the upper layer does not seem to be appropriate, at first glance, so work is still in progress to find a suitable upper-layer generalization of geostrophy.

The bottom topography of the Atlantic Ocean is certainly more complicated than a meridional channel. Although one may argue that the topography may reasonably be modeled as a meridional channel away from the equator, in the vicinity of the equator, the large-scale channel nature disappears, and the local topography is actually better approximated by an east-west channel, see Figure 1. Thus, it remains

for future research to compare the predictions of these models over a realistic bottom topography.

REFERENCES

1. A. Arakawa and Y.-J.G. Hsu, *Energy conserving and potential-enstrophy dissipating schemes for the shallow water equations*, Mon. Wea. Rev. **118** (1990), 1960–1969.

2. S. Borisov and D. Nof, *Deep, cross-equatorial eddies*, Geophys. Astrophys. Fluid Dyn. **87** (1998), 273–310.

3. A. Colin De Verdière and R. Schopp, *Flows in a rotating spherical shell: The equatorial case*, J. Fluid Mech. **276** (1994), 233–260.

4. X.D. DeMadron and G. Weatherly, *Circulation, transport and bottom boundary layers of the deep currents in the Brazil Basin*, J. Mar. Res. **52** (1994), 583–638.

5. N.R. Edwards, A.J. Wilmott and P.D. Killworth, *On the role of topography and wind stress on the stability of the thermohaline circulation*, J. Phys. Oceanogr. **28** (1998), 756–778.

6. C.A. Edwards and J. Pedlosky, *Dynamics of nonlinear cross-equatorial flow*, Part I: *Potential vorticity transformation*, J. Phys. Oceanogr. **28** (1998), 2382–2406.

7. ———, *Dynamics of nonlinear cross-equatorial flow*, Part II: *The tropically enhanced instability of the western boundary current*, J. Phys. Oceanogr. **28** (1998), 2407–2417.

8. M.A.M. Friedrichs and M.M. Hall, *Deep circulation in the tropical North Atlantic*, J. Mar. Res. **51** (1993), 697–736.

9. Y.-J.G. Hus and A. Arakawa, *Numerical modeling of the atmosphere with an isentropic vertical coordinate*, Mon. Wea. Rev. **118** (1990), 1933–1959.

10. G. Johnson, *A deep inertial jet on a sloping bottom near the equator*, Deep-Sea Res. **40** (1993), 1781–1792.

11. R.H. Karsten and G.E. Swaters, *A unified asymptotic derivation of two-layer frontal geostrophic models including planetary sphericity and variable topography*, Phys. Fluids **11** (1999), 2583–2597.

12. M. Kawase, L.M. Rothstein and S.R. Springer, *Encounter of a deep western boundary current with the equator: A numerical spin-up experiment*, J. Geophys. Res. **97** (1992), 5447–5463.

13. M. Kawase and D. Straub, *Spinup of source-driven circulation in an abyssal basin in the presence of bottom topography*, J. Phys. Oceanogr. **21** (1991), 1501–1514.

14. T. Matsuno, *A finite difference scheme for time integrations of oscillatory equations with second order accuracy and sharp cut-off for high frequencies*, J. Meteor. Soc. Japan **44** (1966), 85–88.

15. D. Nof, *The translation of isolated cold eddies on a sloping bottom*, Deep-Sea Res. **30** (1983), 171–182.

16. D. Nof and S. Borisov, *Inter-hemispheric oceanic exchange*, Q. J. R. Meteorol. Soc. **124** (1998), 2829–2866.

17. D. Nof and D.B. Olson, *How do western abyssal currents cross the equator?*, Deep-Sea Res. **40** (1993), 235–255.

18. J. Pedlosky, *Geophysical fluid dynamics*, Springer-Verlag, New York, 1987.

19. R.M. Samelson, *Large-scale circulation with locally enhanced vertical mixing*, J. Phys. Oceanogr. **28** (1998), 712–726.

20. R.M. Samelson and G.K. Vallis, *A simple friction and diffusion scheme for planetary geostrophic basin models*, J. Phys. Oceanogr. **27** (1997), 186–194.

21. J.C. Stephens and D.P. Marshall, *Dynamical pathways of Antarctic bottom water in the Atlantic*, J. Phys. Oceanogr. **30** (2000), 622–640.

22. G.E. Swaters and G.R. Flierl, *Dynamics of ventilated coherent cold eddies on a sloping bottom*, J. Fluid Mech. **223** (1991), 565–587.

College of Oceanic and Atmospheric Sciences, Oregon State University, Corvallis, Oregon, USA
E-mail address: pchobote@coas.oregonstate.edu

Applied Mathematics Institute, Department of Mathematical Sciences, and Department of Earth and Atmosheric Sciences, University of Alberta, Edmonton, Alberta, Canada
E-mail address: gordon.swaters@ualberta.ca